A Selective Blocking Method To Control the Overgrowth of Pt on Au Nanorods

John Fennell,[†] Dongsheng He,[‡] Anicetus Muche Tanyi,[†] Andrew J. Logsdail,[†,§] Roy L. Johnston,[†] Z. Y. Li,*[,‡] and Sarah L. Horswell*[,†]

[†]School of Chemistry, University of Birmingham, Edgbaston, Birmingham B15 2TT, U.K.

[‡]Nanoscale Physics Research Laboratory, School of Physics and Astronomy, University of Birmingham, Edgbaston, Birmingham B15 2TT, U.K.

Ⓢ *Supporting Information*

ABSTRACT: A method for the preparation of smooth deposits of Pt on Au nanorods is described, involving sequential deposition steps with selective blocking of surface sites that reduces Pt-on-Pt deposition. The Au−Pt nanorods prepared by this method have higher long-term stability than those prepared by standard Pt deposition. Electrochemical data show that the resulting structure has more extended regions of Pt surface and enhanced activity toward the carbon monoxide oxidation and oxygen reduction reactions.
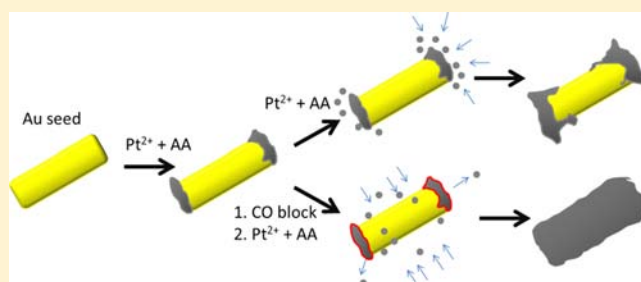
INTRODUCTION

There has been extensive study of metallic nanoparticles as a result of the interesting properties that can arise at short length scales.[1,2] Advances in synthesis have allowed the preparation of gold nanoparticles with good control over size and shape, affording opportunities to understand the effect of these parameters on their properties.[3−6] Bimetallic systems provide further means to tune the properties of nanoparticles through variation of composition and chemical ordering within the nanoparticles.[7] In particular, Au−Pt and Au−Pd nanoparticle systems have attracted interest because of their potential applications as catalysts, and the composition and distribution of the two metals have been shown to impact on their activity and selectivity.[8−11]

Theoretical calculations suggest that for Au−Pt systems, a Pt core with a Au shell should be the most thermodynamically stable arrangement at the nanoscale. Despite this, it has been possible both to synthesize alloyed Au−Pt nanoparticles and to deposit Pt onto Au seed nanoparticles to produce Au nanoparticles with Pt shells.[12] However, the formation of a smooth Pt overlayer on Au is difficult; for example, small Pt particles form on the surface of Au nanorods (NRs). Similarly, growth of Rh on Au NRs is uneven.[13] In contrast, however, Pd easily forms smooth layers on Au.[14] This could result from a number of factors, including the high surface and cohesive energies of Pt (2.49 J m^{-2} and 5.48 eV/atom, respectively).[15] For bulk systems, it is possible to form monolayers of Pt on Au through galvanic displacement of Cu monolayers deposited by underpotential deposition (UPD),[16,17] although UPD of Cu monolayers is less straightforward at the nanoscale.[18] There are few studies on the stability of Au−Pt core−shell particles, although a recent paper showed that the structure of Au NRs

with Pt shells alters over time or upon annealing.[19] The incomplete coverage of Au by Pt may provide channels for Au diffusion to the outside of the nanoparticle. The purpose of the present study was to develop a method of forming smoother, more complete coatings of Pt on Au NRs both to enhance the stability of the core−shell structure and to determine the impact on electrocatalytic performance. We show that a method involving sequential deposition using selective blocking can be successfully employed to produce Au core−Pt shell NRs with considerably enhanced stability and catalytic activity.

EXPERIMENTAL SECTION

Au NRs were synthesized using the method reported by Nikoobakht and El-Sayed.[20] Platinum was deposited onto the Au NRs at a Au:Pt molar ratio of 1:0.5 by modification of the method of Grzelczak et al.[21] (details are provided in the Supporting Information). Additional Pt was deposited onto samples of Au−Pt NRs to give a total Au:Pt ratio of 1:1. One sample was subjected simply to further deposition with the same quantity of Pt salt. A second sample was first bubbled with carbon monoxide for 30 min, left to stand for 1 h, and then bubbled with Ar for 40 min before the second deposition of Pt was performed. The idea behind the additional step in the procedure was to block some of the Pt sites with CO (which binds more strongly to Pt than to Au) in order to encourage further Pt deposition to take place on exposed Au sites. For electrochemical measurements, Au or Au−Pt NRs were dispersed on carbon powder and deposited on a glassy carbon rotating-disk electrode (RDE) using Nafion as a binder. The residual surfactant on the NR surfaces was removed by an electrochemical cleaning procedure as described in the Supporting Information.
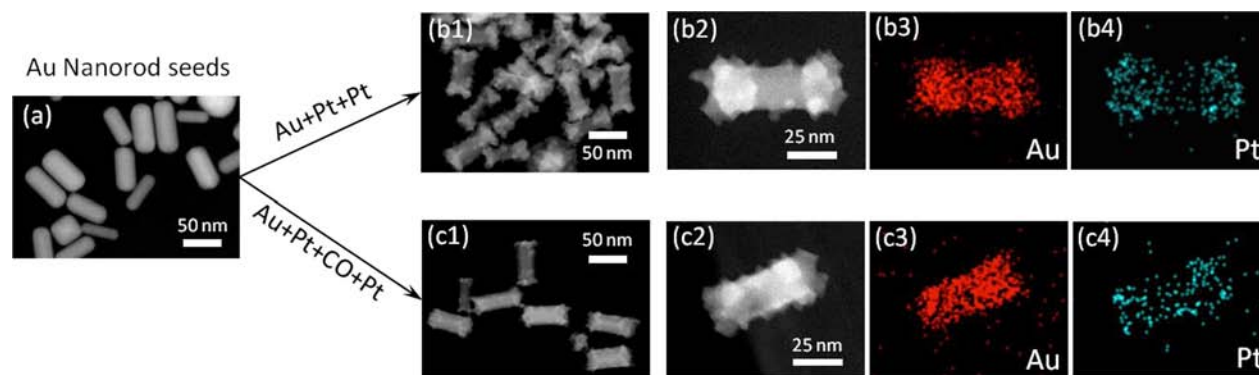
Figure 1. HAADF-STEM images of (a) Au NRs, (b1, b2) Au−Pt NRs prepared without the CO blocking step, and (c1, c2) Au−Pt NRs of same composition prepared with the CO blocking step. Also shown are EDX maps of the (b3, c3) Au and (b4, c4) Pt distributions in the NRs from (b2) and (c2), respectively. Images (b2−b4) and (c2−c4) share the same scale bar.

■ RESULTS AND DISCUSSION

High-angle annular dark-field scanning transmission electron microscopy (HAADF-STEM) images of the NRs are presented in Figure 1. The Au rods have an average width of 23.5 nm and an average length of 59.2 nm, giving an aspect ratio of 2.6 ± 0.5. They are smooth in appearance and have rounded ends. The first deposition of Pt mainly results in deposition at the ends of the rods. The tendency of Pt to deposit at ends has been discussed previously.[12] It could arise from blocking of the sides of the NRs by bromide or underpotentially deposited Ag, higher surface energy of the rod end facets compared with the side facets, or enhanced mass transport of platinum precursor to the ends of the rods (hemispherical diffusion compared with planar diffusion conditions). In addition, once Pt has nucleated on the rods, there is a thermodynamic preference for additional Pt to grow on Pt rather than on exposed Au because of the higher cohesive and surface energies of Pt as well as the lattice strain (~3.9%) caused by the mismatch in lattice parameters (Table 1).[19]

Table 1. Summary of Key Parameters of Au and Pt for Comparison[a]

	Au	Pt
fcc lattice parameter (Å)	4.08	3.92
atomic radius (Å)	1.74	1.77
surface energy (J m^{-2})	1.50	2.49
cohesive energy (eV atom^{-1})	3.81	5.48

[a]Data were taken from refs 22 and 23.

When additional Pt is deposited, the Pt does indeed continue to grow more at the ends of the rods, as shown in Figure 1b. Figure 1c shows that the second deposition is more even when the first layer of Pt is blocked by CO. The Au−Pt rods are smoother in Figure 1c1 than in Figure 1b1, and the contrast is more even across the rod. Au and Pt have similar atomic numbers, which means that contrast observed in the images is mainly related to the thickness. Panels b2 and c2 in Figure 1 are higher-magnification images of a typical NR from each sample, and energy-dispersive X-ray analysis (EDX) maps of the Au and Pt distributions for each sample are presented in panels b3,4 and c3,4, respectively. The EDX maps show that the standard Au−Pt NR samples have greater Pt concentration at the ends of NRs (Figure 1b4), whereas the samples prepared with selective blocking by CO have a more even Pt distribution, with more Pt

in the middle of the rod (Figure 1c4). Measurements of the mean aspect ratios and indications of the degrees of outgrowth at the corners are shown in Figure 2 (lengths and widths are
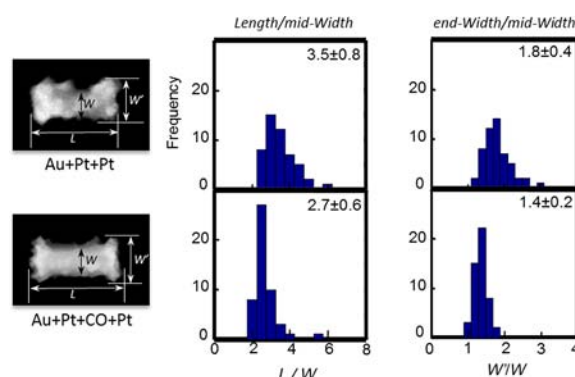

Figure 2. Mean aspect ratios and degrees of outgrowth of Au and Au−Pt NR samples.

provided in the Supporting Information). The mean aspect ratio of the Au−Pt NRs prepared by selective blocking (2.7 ± 0.6) is close to that of the original Au NRs, whereas that of NRs prepared without selective blocking is higher (3.5 ± 0.8), indicating preferential growth of Pt at the ends when the existing Pt deposits are not blocked. In addition, there is a greater propensity for Pt to grow on the corners than on the ends or the sides of the rods. These elemental mapping and morphological observations all indicate that CO blocking is effective in producing a more even distribution of Pt on the Au NR seeds.

Images acquired for the samples after 5 and 17 months (Figure S2 in the Supporting Information) showed that Au−Pt NRs prepared without a blocking step underwent significant morphological changes, akin to those reported previously for similar samples.[19] In contrast, NRs prepared with the selective blocking method retained their original size and shape. Hence, the blocking method produces Au−Pt core−shell NRs that exhibit greater long-term stability than NRs obtained by standard chemical deposition.

Figure 3 presents UV−vis spectra of Au NRs and Au NRs coated with Pt. Two absorption peaks are observed, corresponding to localized surface plasmon resonances in the transverse (TSPR) and longitudinal (LSPR) directions.[24] As Pt is deposited onto the NRs, the LSPR peak is red-shifted and
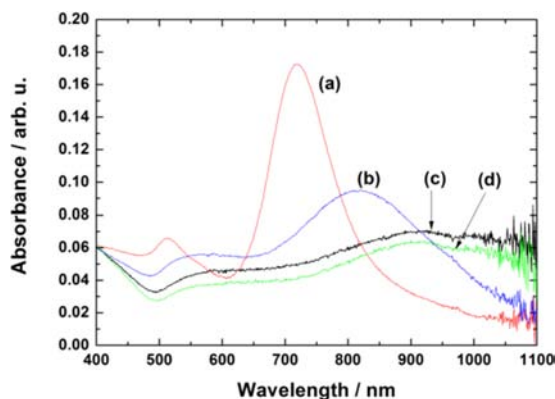
Figure 3. UV−vis absorption spectra of Au and Au−Pt NR samples: (a) Au; (b) Au−Pt (1:0.5); (c) Au−Pt (1:1) prepared without the CO blocking step; (d) Au−Pt (1:1) prepared with the CO blocking step.

broadened, in line with previous observations for deposition of transition metals onto NRs.[12,13] The TSPR peak is often less sensitive to the deposition of metals, and this is observed also in Figure 3. The red shift is usually related to an increase in the aspect ratio of the NR.[24]

We confirmed these observations via computational simulation using the discrete dipole approximation,[25] as implemented in the software package DDSCAT[26] (further details concerning the DDSCAT configuration and calibration are given in the Supporting Information, and calculated spectra are shown in Figures S3−S6). A cylindrical Au NR was constructed with aspect ratio close to those of the NRs shown in Figure 1a: the rod length (L) was set to 30 nm, and the radius was set to 5 nm, giving a width (W) of 10 nm and an aspect ratio ($AR = L/W$) of 3. The incoming radiation was set at an angle of 45° relative to the principal axis of the NR, ensuring excitation of both the TSPR and LSPR modes, as appropriate. The calculated λ_{max} for the Au NR was ∼630 nm, which is a little lower than that in the experimental spectrum (Figure 3), but there is dispersion in the experimental aspect ratios. It is well-known from experiment and calculations that increasing the AR in homogeneous Au NRs results in a red shift of the LSPR;[27] this is verified in Figure S6 in the Supporting Information, which shows calculated spectra for Au NRs with ARs of 3−5.

Calculations of extinction spectra for nonhomogeneous models of NRs are not widely seen in the literature. By adding Pt deposits at the ends of the Au NR (in a "capping" position; Figure 4a middle) and on the sides of the Au NR (in what we have named a "coating" position; Figure 4a right), we were able to calculate the effect of Pt deposition on the optical extinction spectrum. Figure 4b shows the extinction spectra for a bare Au NR (L = 30 nm, W = 10 nm, AR = 3), a Pt-capped Au NR with cap thickness θ = 5 nm (overall AR = 4), and Au NRs with initial Pt caps (θ_1 = 5 nm) and then a secondary Pt capping and coating (i.e., a universal covering) with a thickness of 1 or 2 nm ($\theta_2 = \phi$ = 1 or 2 nm, overall AR = 3.5 or 3.14, respectively), corresponding to the experimentally observed structures. There are multiple changes to the extinction spectrum resulting from the additions of Pt, the predominant factors being the geometric dependence of λ_{max} on the AR[27] and the quenching effects of the Pt dielectric medium.[12] Our calculations (Figure 4b) show a clear red shift of the LSPR from λ_{max} = 627 to 688 nm for the Pt-capped Au NR (AR = 4). The red shift in the
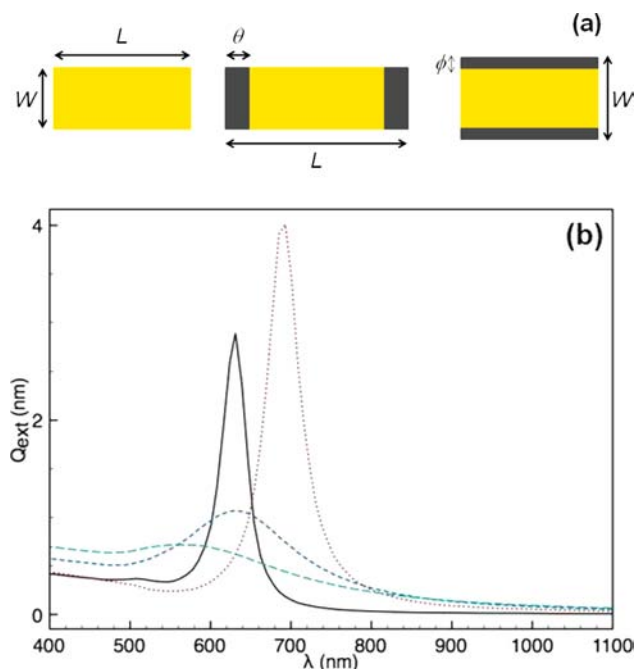

Figure 4. (a) Schematic representations of Au−Pt NR models: (left) bare Au NR with AR = 3 (length L = 30 nm, width W = 10 nm); (middle) Au NR with added Pt caps (thickness θ); (right) Au NR with a Pt coating (thickness ϕ). The angle of the incoming incident radiation relative to the principal (long) axis is 45°. (b) Calculated extinction spectra (Q_{ext}) of Au−Pt NRs over the range 400 nm > λ > 1100 nm. The spectrum for the bare Au NR (AR = 3) is shown by a black solid line. The spectrum for a Pt-capped Au NR (θ = 5 nm, AR = 4) is plotted as a red dotted line. Spectra for geometric models with initial Pt caps (θ_1 = 5 nm) and a secondary Pt capping and coating ($\theta_2 = \phi$ = 1 or 2 nm, AR = 3.5 or 3.14, respectively) are plotted with blue short-dashed and green long-dashed lines, respectively, illustrating clear quenching of the spectral features with increasing Pt coating.

LSPR is not as large as that for a pure Au NR with AR = 4 (Figure S6).

In our experimental spectra (Figure 3), little difference is apparent between the spectra of rods prepared by direct Pt deposition and by deposition onto selectively blocked NRs. Figure 4b shows that Pt coating leads to rapid quenching of the recognizable Au LSPR spectral feature, even for a thickness ϕ of only 1 nm. Blue shifts of the LSPR peaks, resulting from the decrease in AR for these thicker NRs, were also observed. Referring back to our experimental UV−vis spectra, from these calculations we can postulate that the second Pt deposition would need to be prominently on the end of the Pt-capped Au NR to ensure a further red shift in the LSPR peak as seen in Figure 3. Considering the HAADF-STEM images in Figure 1 and the compositional Au:Pt ratio of 1:1 (which would require a Pt coating of between 1 and 2 nm in our model), it seems plausible that the Au LSPR is in fact quenched, resulting in similar spectral signatures for the two samples of higher Pt content [spectra (c) and (d) in Figure 3].

Figure 5 shows cyclic voltammograms (CVs) of carbon-supported Au and Au−Pt NRs in sulfuric acid. In each CV, a pair of redox waves centered at ∼0.3 V vs SCE arises from the redox reactions of functional groups on the carbon surface, most likely quinones.[28,29] The high background current also results from the carbon support.[29] This current is larger for the Au/C sample and decreases as the ratio of accessible Pt surface area to Au surface area increases. In view of the fact that the
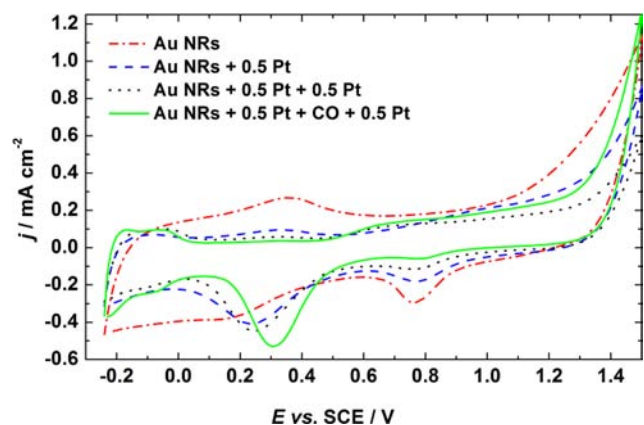
Figure 5. CVs of carbon-supported Au and Au−Pt NR samples in Ar-saturated 0.05 M H_2SO_4. The scan rate was 0.05 V s^{-1}, and the current density (j) is referred to the electrochemically active surface area (see Table 2).

total active surface areas of the catalysts are similar (vide infra), this effect is unlikely to result from differences in loading. The effect is not discussed in the literature, but there is precedent for mixed Au−Pt nanoparticle systems to produce lower capacitive currents at greater Pt:Au surface ratios.[30] The CV of the Au NRs displays a wave at ~0.8 V on the cathodic scan that corresponds to the reduction of gold oxide. This feature is decreased when the Au NRs are coated with Pt. If it is assumed that a charge of 400 μC cm^{-2} is required to reduce gold oxide,[31] the accessible area of Au can be evaluated. Table 2 lists the values of the charge and electrochemically active Au surface area for each sample. The Au−Pt sample prepared by the selective blocking method displayed the smallest gold oxide reduction wave, indicating that the accessible surface area of gold is smallest for this sample.

The wave at ~0.3 V on the negative-going potential sweep corresponds to the reduction of platinum oxide and is indicative of the accessible surface area of Pt. This peak appears to increase in size as more Pt is deposited and also appears to be largest for the sample produced by selective blocking. However, the overlap of this peak with that arising from carbon functional groups precludes its quantitative analysis. The peaks corresponding to metal oxide reduction are a little negative of those obtained for polycrystalline Pt and Au under similar conditions, suggesting slower kinetics for the reduction of these oxides. At the negative limit, hydrogen adsorption and desorption can be observed on the Pt−Au surfaces. The area under the peaks indicates that the surface coverage with Pt is larger for the particles prepared by the selective blocking method. Table 2 also provides values for the samples' active Pt surface areas, obtained by integrating the area under the background-

corrected desorption wave and assuming a charge of 209 μC cm^{-2} for the same reaction on polycrystalline Pt.[32] Under the assumption that the loading of NRs is similar for each experiment, the total surface area for each sample should be similar, and this is indeed observed.

An estimate of the coverage of Au with Pt can be obtained by comparing the Au and Pt areas for each sample. These estimates are provided in Table 2 and show that the sample prepared with selective blocking has the highest coverage of Pt (despite the fact that two samples contain the same Pt:Au molar ratio). The shape of the peaks corresponding to hydrogen desorption provides information on the types of Pt surface sites available. The voltammetric profile for the NRs prepared by selective blocking resembles that of polycrystalline Pt and indicates a high proportion of {110} and {100} step sites on the surface, whereas those of the other two catalysts suggest fewer {110}-type sites.[33,34]

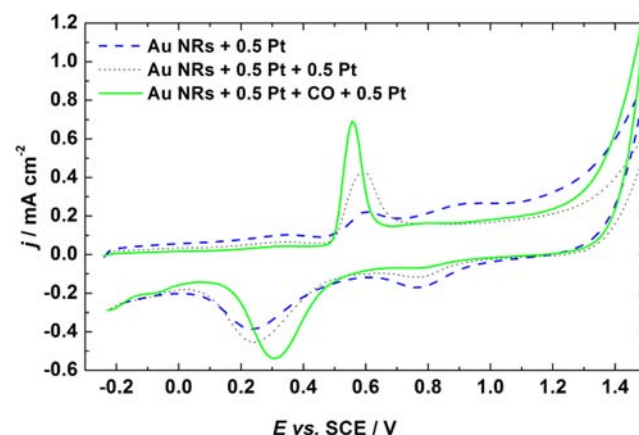CVs comparing the oxidation of adsorbed CO on the three Au−Pt samples are presented in Figure 6. The CO was

Figure 6. CO stripping voltammograms for the carbon-supported catalysts in 0.05 M H_2SO_4 electrolyte. The scan rate was 0.05 V s^{-1}, and the current density is referred to the electrochemically active surface area (see Table 2).

adsorbed at 0.055 V and displaced from solution with Ar before the CVs were recorded. As expected, each CV shows an absence of features relating to hydrogen desorption (CO adsorption blocks hydrogen adsorption on the surface), and a new current peak on the anodic scan is present, which corresponds to the oxidative desorption of CO. Interestingly, the onset potentials of CO oxidation are similar for the three samples. However, the breadth of the peak decreases as the Pt surface area increases. The nanoparticles with the lowest Pt coverage exhibit the lowest activity, with a broad wave followed

Table 2. Charges under the Gold Oxide Reduction Wave and the H_{UPD} Desorption Waves from the CVs in Figure 5, Electrochemically Active Surface Areas of Au and Pt Evaluated from the Charges, and Estimates of the Coverage of Au by Pt and the Au:Pt Ratio

sample	charge under gold oxide reduction wave/μC	electrochemically active area of Au/cm^2	charge under H_{UPD} desorption waves/μC	electrochemically active area of Pt/cm^2	total active area/cm^2	% area Pt	Pt:Au surface area ratio
Au	236	0.59	0	0	0.59	0	0
Au−Pt	184	0.46	31.2	0.15	0.61	24.6	0.33
Au−Pt−Pt	123	0.31	54.6	0.26	0.57	45.6	0.84
Au−Pt−CO−Pt	81.2	0.20	75.6	0.36	0.56	64.3	1.8

by another wave at more positive potentials. The nanoparticles prepared by the selective blocking method produce CVs with a sharp peak centered at more negative potentials, reminiscent of similar measurements on polycrystalline Pt,[35] and with higher overall charge than for CVs of the other samples. The sharpness of the peak, along with the CVs of the clean NR surfaces, indicates that the selective blocking method yields NRs with more extended regions of Pt surface. The higher activity of the particles prepared by selective blocking could also be related to the larger number of {110}-type sites observed in the CV data.[33,36,37]

Rotating-disk electrode polarization curves acquired for the catalysts at a rotation rate of 1600 rpm in O_2-saturated sulfuric acid electrolyte are compared in Figure 7 (full sets of RDE
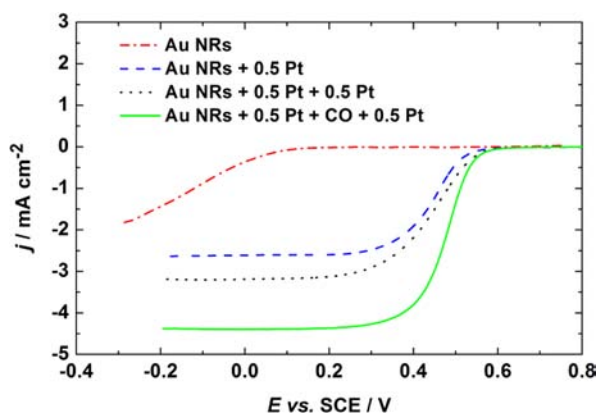

Figure 7. Hydrodynamic voltammograms acquired for carbon-supported catalysts in oxygen-saturated 0.05 M H_2SO_4. The scan rate was 0.002 V s^{-1}, and the rotation rate was 1600 rpm. The current density was calculated from the geometric surface area.

polarization curves at different rotation rates for each catalyst are provided in Figure S6 in the Supporting Information). The shape of the curve observed for Au NRs is similar to those previously reported for Au surfaces[29] and nanoparticles in acidic media and reflects the slow kinetics of oxygen reduction on Au in acidic solutions: the onset of the current is at a significantly more negative applied potential, and the current does not reach a plateau, indicating that the rate of reaction does not reach a point where it is limited by mass transport alone in the potential range employed (i.e., it is limited by both kinetics and mass transport, even at the negative potential limit).

The Pt-coated Au NRs exhibit faster kinetics, in that the RDE curves all reached a mass-transport-limited current at negative potentials and the onset of current was at a much more positive potential than for Au, albeit at a slightly more negative potential than previously reported for carbon-supported ~3 nm diameter Pt particles.[38] It is immediately apparent that the catalyst prepared by the selective blocking method is the most active, as the current in the mixed-control region is significantly higher. The current plateaus in the mass-transport-limited region indicate differing selectivities of the catalysts toward the oxygen reduction reaction (ORR). Oxygen can be reduced via a four-electron reduction to water (directly or in two sequential two-electron steps) or via a two-electron reduction to hydrogen peroxide (Scheme 1).[39,40] The larger current densities observed for the catalyst produced with the selective blocking method indicate that a higher proportion of water is produced as a product in the ORR.

Scheme 1. Oxygen Reduction Pathways to Water and to Hydrogen Peroxide
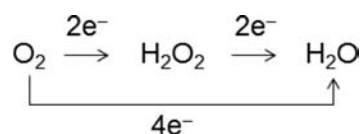
The average number of electrons transferred per oxygen molecule can be evaluated from the data in Figure 7 using the Koutecky−Levich equation:[41]

$$\frac{1}{j} = \frac{1}{j_k} + \frac{1}{j_L}$$

$$= \frac{1}{nFC_a k^0 e^{-[\alpha n_a F(E-E^0)/RT]}} + \frac{1}{0.2006 nF v^{-1/6} C_a D_a^{2/3} \omega^{1/2}}$$

(1)

where j is the current density, j_L is the limiting current density, j_k is the kinetic current density, n is the number of electrons transferred, k^0 is the standard rate constant (referred to the standard potential, E^0), E is the applied potential, R is the gas constant, T is the absolute temperature, α is the transfer coefficient, n_a is the number of electrons transferred in the rate-determining step, F is the Faraday constant, C_a is the bulk concentration of species a and D_a is its diffusivity, v is the kinematic viscosity, and ω is the rotation rate (in rpm). Representative plots of j^{-1} versus $\omega^{-1/2}$ (at an applied potential of −0.1 V) for the catalysts are provided in Figure 8a, along with lines having the slopes expected for four-electron and two-electron reductions. These plots assume an oxygen solubility of 1.26×10^{-6} mol cm^{-3} in the solution, a diffusivity of 1.93×10^{-5} cm^2 s^{-1}, and a kinematic viscosity of 0.01009 cm^2 s^{-1}.[38] From eq 1, values of n as a function of potential can be evaluated, and these data are presented in Figure 8b.

A range of means to compare the activities of catalysts have been reported in the literature. We chose to estimate standard rate constants (referred to the standard potential for reduction of oxygen to water) as well as specific activities at 0.55 V vs SCE, for ease of comparison with other Au-supported Pt systems. To estimate the standard rate constants, data were fitted to eq 1 with Igor Pro using nonlinear regression analysis with E^0 = 1.23 V, n_a = 1, and C_a, D_a, and v as above.

The value of α had to be constrained to 0.5, and n and k^0 were allowed to vary. Each polarization curve was fitted to eq 1, and the values of n and k^0 were averaged. The values of n were found to be similar to those obtained in Figure 8; they are given in Table 3 along with the values of k^0, the latter normalized to the active surface area (estimated as the sum of the electrochemically active areas of Au and Pt in Table 2). The error margins represent standard deviations of the values averaged. The values of the standard rate constant are of similar magnitude, with the catalyst prepared by selective blocking being slightly more active than the other two materials. The main advantage of this catalyst would thus appear to be the larger currents obtained and greater selectivity toward water.

The exchange current density reported for carbon-supported Pt nanoparticles is 1.66×10^{-8} A cm^{-2},[42] corresponding roughly to a rate constant on the order of $(3.7-7) \times 10^{-8}$ cm s^{-1} (depending on the value of n). The rate constants in Table 3 are a little larger than this value. The reason why the rate constants measured for the catalysts in the present work are larger is not obvious, and literature relating to the ORR on Au−
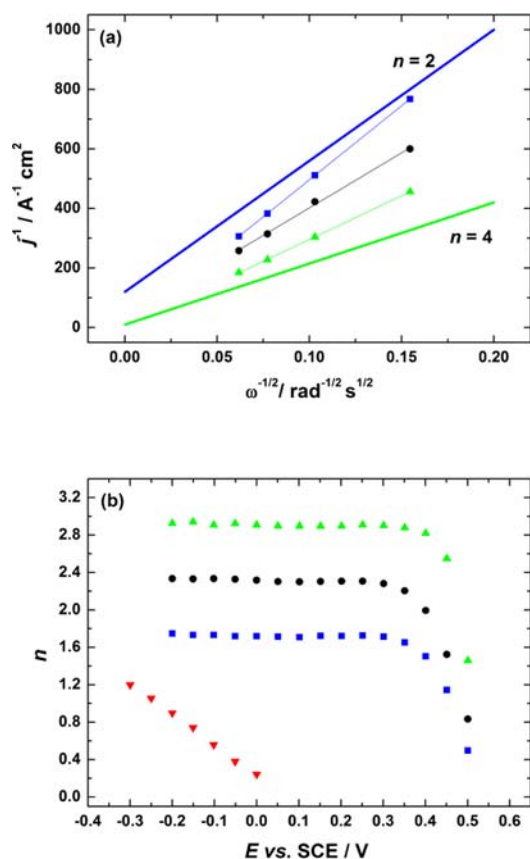
Figure 8. (a) Examples of Koutecky−Levich plots derived from the data in Figure 7 at $E = -0.1$ V. The thick blue and green lines have the theoretical slopes for two- and four-electron pathways, respectively (the two-electron line has been shifted for clarity). (b) Values of the number of electrons transferred (n) as a function of applied potential, derived from the Koutecky−Levich plots: red ▼, Au NRs; blue ■, Au−Pt (1:0.5); black ●, Au−Pt (1:1); green ▲, Au−Pt (1:1) prepared by selective blocking.

Table 3. Numbers of Electrons Transferred (n) and Standard Rate Constants Normalized to Active Surface Area (k^0) Estimated from Nonlinear Regression Analysis Using Equation 1

sample	n	$k^0/cm\ s^{-1}$
Au−Pt	1.74 ± 0.01	$(3.90 \pm 0.81) \times 10^{-7}$
Au−Pt−Pt	2.11 ± 0.08	$(4.42 \pm 0.95) \times 10^{-7}$
Au−Pt−CO−Pt	2.93 ± 0.02	$(8.68 \pm 2.45) \times 10^{-7}$

Pt systems reports various effects: some reports show increased activity relative to Pt[10,30,43,44] and others show lower activity than Pt.[45−47] van Brussel and co-workers reported higher activity for Au-supported Pt in the positive-going sweep (ORR on the reduced surface) but lower activity relative to Pt in the negative-going sweep (ORR on the oxidized surface).[48,49] In the catalyst samples prepared in the present work, Pt was grown epitaxially on the Au NR surface,[19] and the lattice parameters of Au and Pt (4.08 and 3.92 Å, respectively) indicate a strain of 3.9%.[19] Lattice strain has previously been suggested to affect the electronic structure of a metal, shifting its d-band center to higher energy, with the effect that binding of small adsorbates is enhanced.[50,51] Thus, for Au-supported Pt, the adsorption of O_2 would be stronger, enhancing the reaction rate, but the binding of O and OH intermediates is also

predicted to be stronger than on Pt, decreasing the reaction rate. The overall predicted effect is lower ORR activity for Pt/Au(111) compared with Pt(111).[50] In line with this argument, the activities for Au core−Pt shell particles[47] and Au-supported Pt layers[46] displayed a dependence on the thickness of the Pt layer, with thicker deposits approaching the activity of bulk Pt. On the other hand, lattice strain arguments alone do not take into account ligand effects,[50,52] and a recent publication examining the ORR on the (111) and (100) facets suggested that expansion or compression alone is unlikely to be responsible for changes in the binding energies of OH and hence the activity.[53] Some experimental reports indicating increased catalytic activity for Au−Pt systems suggest a synergistic relationship between Au and Pt sites[10,54] and/or a positive shift in the Pt oxidation potential.[10,30]

To compare our data more easily with those for other Au-supported Pt samples, the specific activity (j_k at 0.55 V vs SCE) was obtained from Koutecky−Levich plots and normalized to the electrochemically active surface area and also to the Pt surface area, the latter following Sarapuu et al.[46] At this potential, it was assumed that the activity arose from Pt sites because negligible current was observed for the Au catalysts.[46] The j_k values for our catalysts are presented in Table 4. The

Table 4. Specific Activities (Kinetic Current Densities at 0.55 V vs SCE Obtained from Koutecky−Levich Plots) Normalized to Total Active Surface Area and Normalized to Pt Surface Area

sample	j_k at 0.55 V vs SCE normalized to total active area/A cm^{-2}	j_k at 0.55 V vs SCE normalized to area of Pt/A cm^{-2}
Au−Pt	$(2.3 \pm 0.1) \times 10^{-5}$	$(0.94 \pm 0.6) \times 10^{-4}$
Au−Pt−Pt	$(4.6 \pm 0.4) \times 10^{-5}$	$(1.0 \pm 0.8) \times 10^{-4}$
Au−Pt−CO-Pt	$(8.1 \pm 0.2) \times 10^{-5}$	$(1.3 \pm 0.4) \times 10^{-4}$

Au−Pt 1:1 catalyst prepared without selective blocking exhibits a specific activity (with respect to Pt area) similar to that of the Au−Pt 1:0.5 catalyst; these activities are similar to those reported by Sarapuu et al.[46] for Au-supported Pt deposits catalyzing oxygen reduction in sulfuric acid (for which little dependence of the activity on Pt thickness was observed as a result of the dominating effect of sulfate/bisulfate adsorption).[46] Hence, our two catalysts do not perform worse than bulk systems. The catalyst prepared by selective blocking exhibited ∼25% higher specific activity with respect to Pt area, suggesting that the different morphology of the Pt-on-Au support has an influence on the activity, in line with previous reports.[55] The specific activity observed for this catalyst approaches that reported for bulk (polycrystalline) Pt.[46,56] The increase in current density at this potential is related largely to the increase in the number of electrons transferred, which is higher for the catalyst prepared by selective blocking. Conversion of the current densities to rate constants using the values of n at 0.55 V gives k^0 values of 3.04×10^{-3} and 3.33×10^{-3} cm s^{-1} for the Au−Pt catalysts prepared without and with selective blocking, respectively. These may be compared with the rate constants (normalized to Pt surface area) obtained by van Brussel and co-workers for Pt deposits on Au prepared by displacement of Cu.[48,49] The rate constant for the catalyst prepared by selective blocking is a little higher but has a similar order of magnitude. The main advantage of this catalyst would

thus appear to be the larger specific currents obtained and greater selectivity toward water. Perhaps obtaining a uniform dispersion of Pt over Au rather than concentrating it in particular regions of the NRs enables peroxide generated at Au sites to be reduced at nearby Pt sites, as suggested by Adzic and co-workers.[10]

CONCLUSIONS

A new method for the preparation of smoother films of Pt on Au nanoparticle supports has been described. Sequential deposition with selective blocking of the initial Pt deposits by CO results in a more uniform distribution of Pt on Au nanorods. The catalytic activity of these Au−Pt NRs toward electrochemical oxidation of CO and reduction of oxygen is superior to that of Au−Pt NRs of identical composition but prepared without the blocking steps. The NR structure also has greater long-term stability when prepared with the blocking method. This method could easily be extended to coverage of smaller Au supports and further refined by increasing the number of blocking steps. It could prove useful as a general means of synthesizing Pt (or other transition metal) shell catalysts on nanometallic supports, producing catalysts with enhanced stability and performance.

ASSOCIATED CONTENT

Ⓢ Supporting Information

Experimental details for Au−Pt NR preparation, UV−vis and STEM-HAADF characterization, and electrochemical measurements; additional TEM data, including images of aged NRs and statistics for sizes and shapes of NRs as prepared and after aging; computational methods and results for optical properties of Au−Pt NRs; and RDE polarization curves at all rotation rates for each sample. This material is available free of charge via the Internet at http://pubs.acs.org.

AUTHOR INFORMATION

Corresponding Author

s.l.horswell@bham.ac.uk; z.li@bham.ac.uk

Present Address

§A.J.L.: Kathleen Lonsdale Materials Chemistry, Department of Chemistry, University College London, 20 Gordon St., London WC1H 0AJ, U.K.

Notes

The authors declare no competing financial interest.

REFERENCES

(1) Johnston, R. L. *Atomic and Molecular Clusters*; Taylor and Francis: London, 2002.
(2) Daniel, M.-C.; Astruc, D. *Chem. Rev.* **2004**, *104*, 293−346.
(3) Xia, Y.; Xiong, Y. J.; Lim, B.; Skrabalak, S. E. *Angew. Chem., Int. Ed.* **2009**, *48*, 60−103.
(4) Pérez-Juste, J.; Pastorize-Santos, I.; Liz-Marzán, L. M.; Mulvaney, P. *Coord. Chem. Rev.* **2005**, *249*, 1870−1901.
(5) Sohn, K.; Kim, F.; Pradel, K. C.; Wu, J. S.; Peng, Y.; Zhou, F. M.; Huang, J. X. *ACS Nano* **2009**, *3*, 2191−2198.
(6) Personick, M. L.; Langille, M. R.; Zhang, J.; Mirkin, C. A. *Nano Lett.* **2011**, *11*, 3394−3398.
(7) Ferrando, R.; Jellinek, J.; Johnston, R. L. *Chem. Rev.* **2008**, *108*, 845−910.
(8) Liu, F.; Wechsler, D.; Zhang, P. *Chem. Phys. Lett.* **2008**, *461*, 254−259.
(9) Edwards, J. K.; Hutchings, G. J. *Angew. Chem., Int. Ed.* **2008**, *47*, 9192−9198.
(10) Zhang, J.; Sasaki, K.; Sutter, E.; Adzic, R. R. *Science* **2007**, *315*, 220−222.
(11) Hernández-Fernández, P.; Rojas, S.; Ocón, P.; Gómez de la Fuente, J. L.; San Fabión, J.; Sanza, J.; Peña, M. A.; García-García, F. J.; Terreros, P.; Fierro, J. L. G. *J. Phys. Chem. C* **2007**, *111*, 2193−2923.
(12) Grzelczak, M.; Pérez-Juste, J.; Rodriguez-Gonzalez, B.; Liz-Marzán, L. M. *J. Mater. Chem.* **2006**, *16*, 3946−3951.
(13) Chantry, R. L.; Siriwatcharpiboon, W.; Horswell, S. L.; Logsdail, A. J.; Johnston, R. L.; Li, Z. Y. *J. Phys. Chem. C* **2012**, *116*, 10312−10317.
(14) Song, J. H.; Kim, F.; Kim, D.; Yang, P. D. *Chem.—Eur. J.* **2005**, *11*, 910−916.
(15) Bus, E.; van Bokhoven, J. A. *J. Phys. Chem. C* **2007**, *111*, 9761−9768.
(16) Brankovic, S. R.; Wang, J. X.; Adzic, R. R. *Surf. Sci.* **2001**, *474*, L173−L179.
(17) Zhang, J.; Lima, F. H. B.; Shao, M. H.; Sasaki, K.; Wang, J. X.; Hanson, J.; Adzic, R. R. *J. Phys. Chem. B* **2005**, *109*, 22701−27704.
(18) Price, S. W. T.; Speed, J. D.; Kannan, P.; Russell, A. E. *J. Am. Chem. Soc.* **2011**, *133*, 19448−19458.
(19) He, D. S.; Han, Y.; Fennell, J.; Horswell, S. L.; Li, Z. Y. *Appl. Phys. Lett.* **2012**, *101*, No. 113102.
(20) Nikoobakht, B.; El-Sayed, M. A. *Chem. Mater.* **2003**, *15*, 1957−1962.
(21) Grzelczak, M.; Pérez-Juste, J.; de Abajo, F. J. G.; Liz-Marzán, L. M. *J. Phys. Chem. C* **2007**, *111*, 6183−6188.
(22) Kittel, C. *Introduction to Solid State Physics*, 7th ed.; Wiley: New York, 1996.
(23) Foiles, S.; Baskes, M. I.; Daw, M. S. *Phys. Rev. B* **1986**, *33*, 7983−7991.
(24) Huang, X.; Neretina, S.; El-Sayed, M. A. *Adv. Mater.* **2009**, *21*, 4880−4910.
(25) Purcell, E. M.; Pennypacker, C. R. *Astrophys. J.* **1973**, *186*, 705−714.
(26) Draine, B. T.; Flatau, P. J. *J. Opt. Soc. Am. A* **1994**, *11*, 1491−1499.
(27) Kooij, E. S.; Poelsema, B. *Phys. Chem. Chem. Phys.* **2006**, *8*, 3349−3357.
(28) Alexeyeva, N.; Tammeveski, K. *Electrochem. Solid-State Lett.* **2007**, *10*, F18−F21.
(29) Erikson, H.; Jürmann, G.; Sarapuu, A.; Potter, R. J.; Tammeveski, K. *Electrochim. Acta* **2009**, *54*, 7483−7489.

(30) Hernández-Fernández, P.; Rojas, S.; Ocón, P.; Gómez de la Fuente, J.; San Fabián, J.; Sanza, J.; Peña, M. A.; García-García, F. J.; Terreros, P.; Fierro, J. L. G. *J. Phys. Chem. C* **2007**, *111*, 2913−2923.

(31) Angerstein-Kozlowska, H. In *Comprehensive Treatise of Electrochemistry*, Vol. 9; Yeager, E., Bockris, J. O'M., Conway, B. E., Sarangapani, S., Eds.; Plenum Press: New York, 1984.

(32) Clavilier, J.; Rodes, A.; El Achi, K.; Zamakhchari, M. A. *J. Chim. Phys. Phys.-Chim. Biol.* **1991**, *88*, 1291−1337.

(33) Markovic, N. M.; Marinkovic, N. S.; Adzic, R. R. *J. Electroanal. Chem.* **1991**, *314*, 289−306.

(34) Markovic, N. M.; Grgur, B. N.; Ross, P. N. *J. Phys. Chem. B* **1997**, *101*, 5405−5413.

(35) Esterle, T. F.; Russell, A. E.; Bartlett, P. N. *ChemPhysChem* **2010**, *11*, 2896−2905.

(36) Strmcnik, D. S.; Tripkovic, D. V.; van der Vliet, D.; Chang, K. C.; Komanicky, V.; You, H.; Karapetrov, G.; Greeley, J. P.; Stamenkovic, V. R.; Markovic, N. M. *J. Am. Chem. Soc.* **2008**, *130*, 15332−15339.

(37) Xu, J. Z.; Yates, J. T. *J. Chem. Phys.* **1993**, *99*, 725−732.

(38) Higuchi, E.; Adachi, K.; Nohara, S.; Inoue, H. *Res. Chem. Intermed.* **2009**, *35*, 985−995.

(39) Damjanovic, A.; Genshaw, M. A.; Bockris, J. O'M. *J. Chem. Phys.* **1966**, *45*, 4057−4059.

(40) Markovic, N. M.; Ross, P. N. *Surf. Sci. Rep.* **2002**, *45*, 121−229.

(41) Bard, A. J.; Faulkner, L. R. *Electrochemical Methods: Fundamentals and Applications*; Wiley: New York, 1980.

(42) Stassi, A.; D'Urso, C.; Baglio, V.; Di Blasi, A.; Antonucci, V.; Arico, A. S.; Luna, A. M. C.; Bonesi, A.; Triaca, W. E. *J. Appl. Electrochem.* **2006**, *36*, 1143−1149.

(43) Liu, C. W.; Wei, Y. C.; Wang, K. W. *J. Colloid Interface Sci.* **2009**, *336*, 654−657.

(44) Dešić, M. N.; Popović, M. M.; Obradović, M. D.; Vračar, L. M.; Grgur, B. N. *J. Serb. Chem. Soc.* **2005**, *70*, 231−242.

(45) Maye, M. M.; Kariuki, N. N.; Luo, J.; Han, L.; Njoki, P.; Wang, L.; Lin, Y.; Naslund, R.; Zhong, C. J. *Gold Bull.* **2004**, *37*, 217−224.

(46) Sarapuu, A.; Kallip, S.; Kasikov, A.; Matisen, L.; Tammeveski, K. *J. Electroanal. Chem.* **2008**, *624*, 144−150.

(47) Zhai, J.; Hunag, M.; Dong, S. *Electroanalysis* **2007**, *19*, 506−509.

(48) van Brussel, M.; Kokkinidis, G.; Vandendael, I.; Buess-Herman, C. *Electrochem. Commun.* **2002**, *4*, 808−813.

(49) van Brussel, M.; Kokkinidis, G.; Hubin, A.; Buess-Herman, C. *Electrochim. Acta* **2003**, *48*, 3909−3919.

(50) Zhang, J.; Vukmirovic, M. B.; Xu, Y.; Mavrikakis, M.; Adzic, R. R. *Angew. Chem., Int. Ed.* **2005**, *44*, 2132−2135.

(51) Mavirkakis, M.; Hammer, B.; Nørskov, J. K. *Phys. Rev. Lett.* **1998**, *81*, 2819−2822.

(52) Kitchin, J. R.; Nørskov, J. K.; Barteau, M. A.; Chen, J. G. *J. Chem. Phys.* **2004**, *120*, 10240−10246.

(53) Viswanathan, V.; Hansen, H. A.; Rossmeisl, J.; Nørskov, J. K. *ACS Catal.* **2012**, *2*, 1654−1660.

(54) Luo, J.; Njoki, P. N.; Lin, Y.; Wang, L.; Zhong, C. J. *Electrochem. Commun.* **2006**, *8*, 581−587.

(55) Sleightholme, A. E. S.; Wilkinson, D. P.; Bizzotto, D.; Ye, S.; Gyenge, E. L. *Electrocatalysis* **2010**, *1*, 22−27.

(56) Sarapuu, A.; Kasikov, A.; Laaksonen, T.; Kontturi, K.; Tammeveski, K. *Electrochim. Acta* **2008**, *53*, 5873−5880.